nature communications

Article

https://doi.org/10.1038/s41467-025-57337-0

Impact-induced ultra-high melting point oldhamite discovered in Chang'E-6 lunar soil

Received: 4 October 2024

Accepted: 19 February 2025

Published online: 04 March 2025

Check for updates

Chen Li[1,2], Yang Li[1,3] ✉, Ronghua Pang[1], Jiyang Xie[4], Zixuan Han[1], Yuanyun Wen[1], Xiaojia Zeng[1], Li Wang[2], Ziyan Qin[2], Jie Yang[4], Wanbiao Hu[4], Jianzhong Liu[1,3], Xiongyao Li[1,3] & Wenhui Ma[2]

Chang'E-6 lunar soil was the first sample collected on the lunar farside. It provides insights into impact history and thermodynamic evolution of the Moon. Here we show the discovered widespread oldhamite (CaS) in lunar regolith samples. Analysis of the microscopic composition and crystal structure showed that the oldhamite has a cubic structure and presence at the interface of glass and iron on the surface of the impact glass beads, suggesting a interface thermochemical reaction. Thermodynamic calculations show that the formation of chemical reactions requires a reducing atmosphere and high temperature to ensure reducing environment and high iron activity for promoting the interaction. Such environment suggests a potential large-scale, high-energy impact event with a S-rich asteroid or involving lunar S-rich mantle-core excavation. Oldhamite has never been observed in other lunar samples from near side. Our findings reveal a unique evolution history of the South Pole-Aitken basin, which is distinct from nearside.

The Chang'E-6 lunar soil samples are the first samples collected on the far side of the moon. They contain significant information on the formation and evolution of the moon and the transformation of the space environment. Chang'E-6 landed at 153.978°W, 41.625°S on the far side of the moon. The landing area is located in the southern plains near the Apollo basin northeast of the South Pole-Aitken (SPA) basin, which has multiple terrane sources[1]. The Chang'E-6 lander collected ~1935.3 g of lunar soil using scooping and drilling[2]. The sampling area has multiple terrane sources and may have undergone multiple phases of transformation. Sample analysis is expected to solve key issues, such as the bisection of lunar surface terranes[3]. Multiple stages of magma transformation and an evolutionary period of 2.4-3 billion years[4,5] indicate that the Chang'E-6 lunar soil samples underwent complex thermal transformation.

Different from the formation environment of meteorites, the complex impact environment on the lunar surface substantially changes the physical and chemical properties of lunar soil due to high-temperature and high-pressure effects, producing minerals or microstructures and preserving in the lunar soils. For example, the high-temperature and high-pressure environment generated by the impact can cause the phase change of quartz[6]. Vapor deposition during the impact forms new minerals or microstructures, such as hapkeite[7], nanophase iron (np-Fe^0)[8], and digenite[9]. The chemical processes and redox changes induced by the impact cause valence state changes in the Fe-rich components, resulting in the accumulation of Fe^{3+} [10], np-Fe^0 from disproportionation reactions[11], in-situ thermal reduction[12,13], redeposition from impact vapor[8], and magnetite from eutectoid reactions[14]. Thermal events during the impact can also cause mineral decomposition reactions of heat-sensitive minerals such as fayalite[15] and troilite[16]. Therefore, impact events have changed the thermal environment on the lunar surface. These complex thermal environments have greatly changed the lunar surface, especially the largest SPA basin impact, which may directly affect the lunar mantle and even the lunar core[17,18]. Therefore, the lunar soil samples of Chang'E-6 may reveal potential typical impact products of mantle or core sources.

Minerals with different melting points respond to different thermal events[19,20]. Calcium sulfide (CaS, oldhamite) with a cubic structure (Fm3m) is a sulfide with a high melting point of 2798 K[21]. Oldhamite

[1]Center for Lunar and Planetary Sciences, Institute of Geochemistry, Chinese Academy of Sciences, Guiyang, China. [2]School of Engineering, Yunnan University, Kunming, China. [3]Center for Excellence in Comparative Planetology, Chinese Academy of Sciences, Hefei, China. [4]Electron Microscopy Center, Yunnan University, Kunming, China. ✉e-mail: liyang@mail.gyig.ac.cn

usually exists in enstatite chondrites and some other undifferentiated meteorites, forming in a highly reducing environment[22–24]. It is found in meteorites as individual crystals, coexisting with other sulfides such as ninengerite and heideite[25]. Anomalous distribution of light rare earth elements and S isotope studies in meteorite oldhamite suggest its formation chemical reduction and thermal history[26–28]. Highly reducing conditions are necessary for the formation of oldhamite, and low oxygen partial pressure promotes the formation of sulfides[29]. Experiments have also shown that oldhamite is most stable under low oxygen partial pressure conditions, a property that is important evidence of its presence in such meteorites[30].

Oldhamite is rarely found in natural deposits on the surface or can be produced in the high-temperature, high-pressure mantle condition of the terrestrial planets like Earth and Moon[31]. Calcium sulfide with a stable crystal structure has not yet been found in lunar soil, and only some studies have found sulfides with similar chemical compositions[32–34]. It is unclear whether sulfide minerals with high melting points exist on the lunar surface and which environments they indicate. The newly discovered oldhamite in the samples collected in the Chang'E-6 mission has provided new insights for the evolution history of the Moon.

Results

Iron beads in the impact glass in the Chang'E-6 lunar soil samples

The Chang'E-6 lunar soil contains a wide variety of impact glass and aggregates[2,35]. We found metallic iron particles embedded in the surface of impact glass beads. The particle size of the metal particles ranged from a few hundred nanometers to a few microns. As shown in Fig. 1, the metal particles are uniformly embedded in the surface of the glass beads. More than 1000 particles were searched in the Chang'E-6 lunar soil, and 7 impact glasses of the same occurrence and 15 nanocrystals of oldhamite were found (Supplementary Fig 1). The partially enlarged image shows holes previously occupied by iron particles. Exfoliated holes are uncommon in the lunar regolith, especially in impact glass and metal particles originating from an impact dispersion, because the solidification temperature of iron is higher than the softening temperature of glass[36,37].

The focused ion beam (FIB) slice position and cross-sectional structure of the embedded metal particles are shown in Fig. 2a, b. The cross-section covers multiple metal particles. The FIB cross-section shows the microstructure of the glass beads and metal balls. The glass is uniform indicating that the glass was formed at a relatively high temperature. The metal particles are only embedded on the surface of the glass, suggesting that the metal particles were deposited on the outside of the glass as a gas or liquid. As shown in Fig. 2c–e and Supplementary Fig. 2, a new phase, oldhamite, occurs between the elemental iron particles and the glass beads. Since the atomic mass of CaS is low, the contrast was adjusted to observe it in the high-angle annular dark field (HAADF) image. Low-melting-point sulfides, such as troilite, may exist in the elemental iron-glass phase, but oldhamite has never been found. Therefore, the formation process of the impact glass beads and other glass and iron particles in the lunar soil may be significantly different. Figure 2f, g shows a solar wind damage layer (SW layer) with a thickness of about 100 nm on the surface of the metallic iron. The SW layer has a dense pore structure, and the pore diameter decreases from the surface to the inside. The fast Fourier transform (FFT) image shows that the matrix where the vesicles are located has the crystal structure of α-iron. The vesicles on the metal surface indicate that the particles on the lunar surface had a long history of space exposure, and the solar wind components tend to be saturated[38].

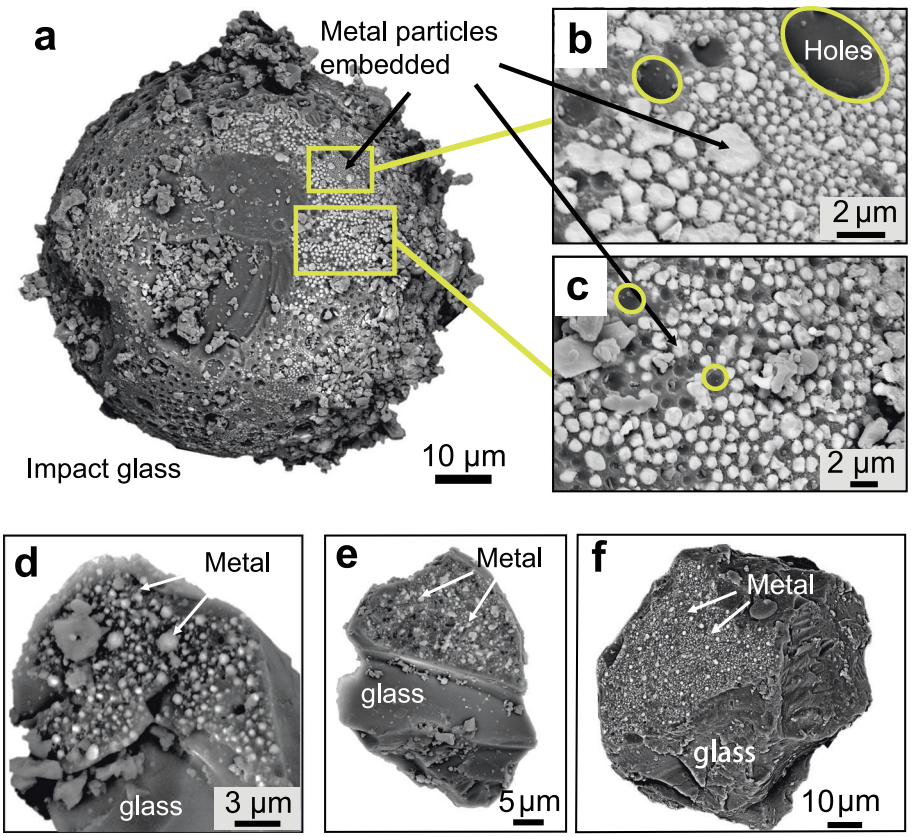

Fig. 1 | SEM images of Chang'E-6 lunar soil impact glass. a Microscopic image of glass beads (metal particles are marked). **b**, **c** Local magnified images of glass beads (holes are marked; The yellow rectangles in (**a**) represent the positions of (**b**, **c**) respectively.). **d**–**f** Typical occurrence of lunar soil impact glass containing oldhamite (metal particles embedded in impact glass).

https://doi.org/10.1038/s41467-025-57337-0

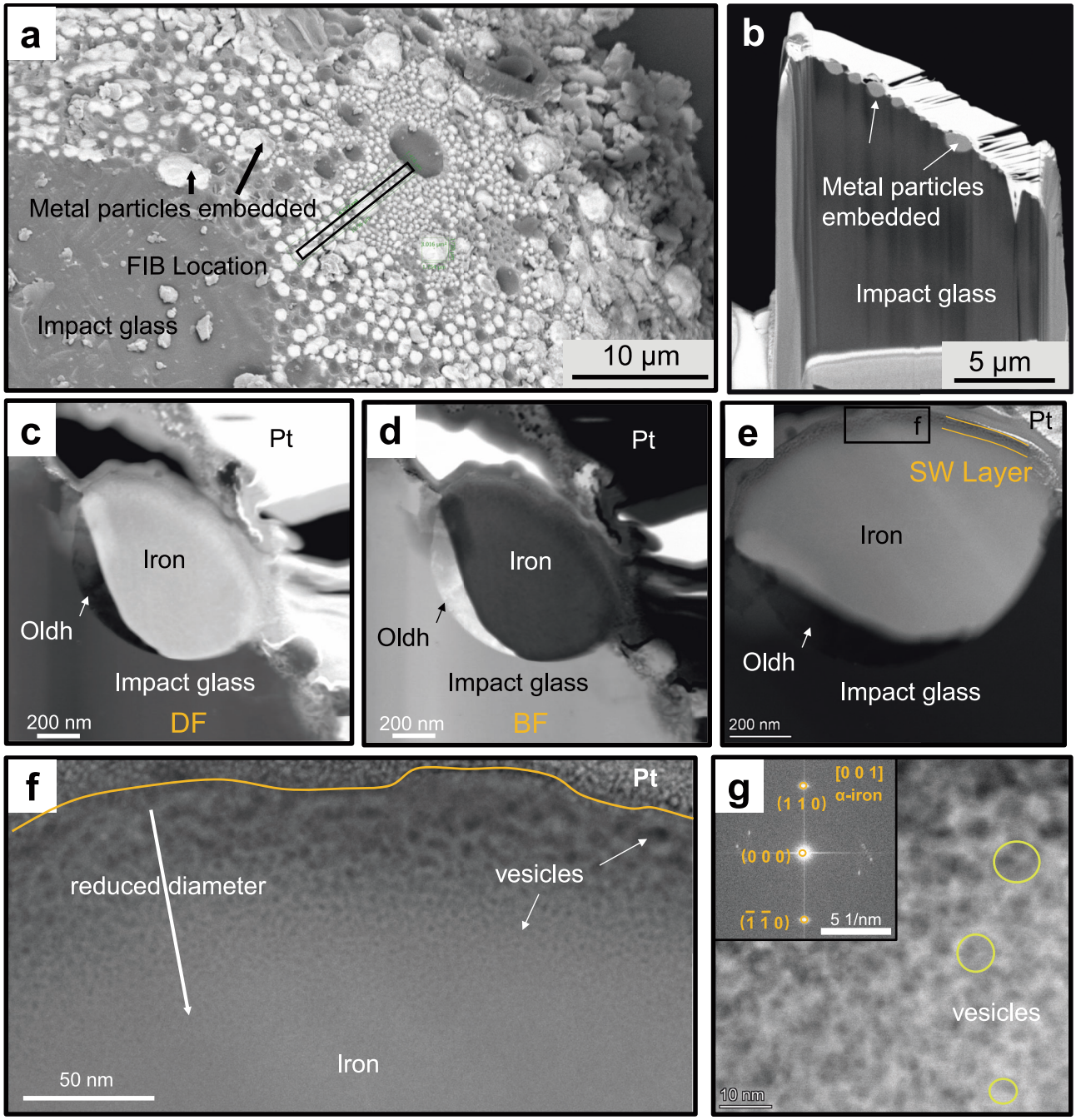

Fig. 2 | FIB slice images and space weathering rim of metal particles embedded in lunar soil impact glass. a FIB slice position; **b** STEM image of the FIB area; **c**, **d** TEM DF and BF images of the interface between iron particles and glass (The Oldh means Oldhamite; orange DF and BF represent the imaging in dark field and bright field modes); **e** HAADF image of the iron particle area containing space weathering rim (The orange SW layer and the curve represent weathered rims); **f**, **g** Vesicles, magnified image, and FFT image of the space weathering rim on the surface of iron (The orange line marks the boundary between the metal phase and the Pt coating).

Composition characteristics and occurrence of oldhamite

Figure 3 shows the results of transmission electron microscopy (TEM), energy dispersive spectroscopy (EDS), and electron energy-loss spectroscopy (EELS) of the oldhamite region, depicting the element composition and distribution. The EDS mapping results of the bright-field (BF) and HAADF images of the same region are shown in Fig. 3a–c. The oldhamite region is enriched with Ca and S, the metal phase does not contain S, and the glass contains calcium (Supplementary Fig. 3). The EDS line scan results (Fig. 3d) also show that the S and Ca ratio in the oldhamite is close to 1 (excluding background elements), and the chemical composition is CaS. In addition, the line scan data indicate S depletion in the metal phase and the loss of Ca in the glass. The atomic-level HAADF image shows the crystal structure of oldhamite (Fig. 3e–g). The hypothetical atomic structure has a high degree of match with the atomic phase, indicating that oldhamite formed under favorable crystallization conditions. The full diffraction of the FFT image also shows that all crystal axes of oldhamite are well crystallized without dislocations and other crystal defects. Oldhamite crystals with an ideal structure have never been found in the lunar soil. Oldhamite has a cubic Fm3m structure and an ultra-high melting point of 2798 K[21], making it the mineral with the highest melting point discovered in the lunar soil. The EELS results

https://doi.org/10.1038/s41467-025-57337-0

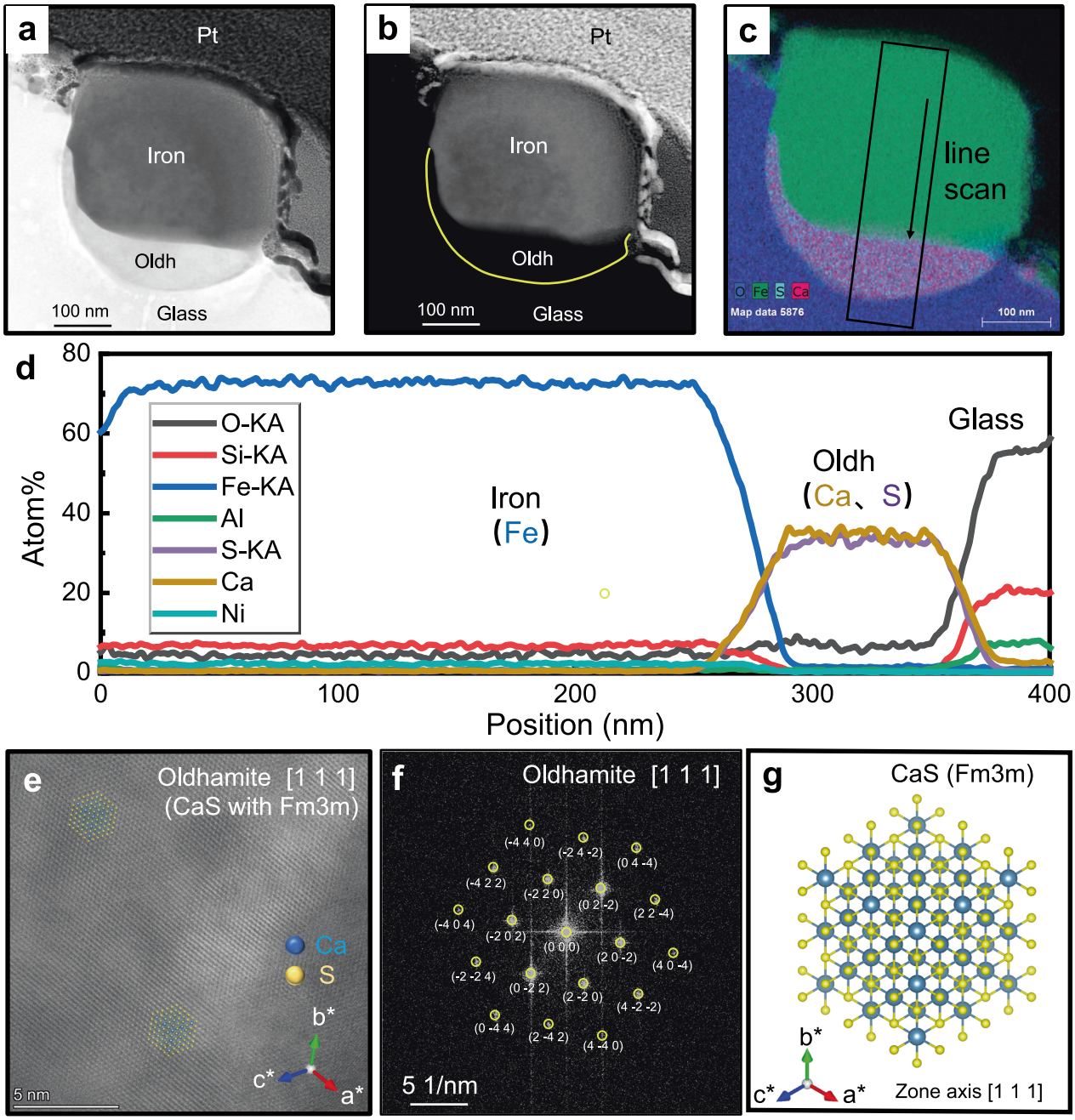

Fig. 3 | TEM images and chemical composition of oldhamite. a, **b** Bright field (BF) and HAADF images of oldhamite (Oldhamite marked as Oldh); **c** Multi-element EDS mapping of the area with oldhamite (In EDS mapping: blue is O, green is Fe, light blue is S, and red is Ca.; the line scan position is marked); **d** EDS line-scan results of the marked area of oldhamite, showing the elemental composition; **e** Atomic-level HAADF image of oldhamite under TEM (the crystal zone axis and atomic configuration are shown); **f** FFT image of the atomic phase of oldhamite (the total diffraction is shown); **g** Crystallographic model of CaS with Fm3m structure(The blue sphere is Ca and the yellow sphere is S).

show that Ca and S are only enriched at the location with the oldhamite (Supplementary Fig. 4). The matrix of the glass is composed of the most common pyroxene-plagioclase impact glass in lunar soil, and sulfur is enriched in the metal phase. The phase located at the interface between the metal phase and the impact glass indicates that oldhamite may originate from liquid-phase interfacial chemical reactions at high temperatures.

As shown in Fig. 4a–d and Supplementary Figs. 2–4, oldhamite is common at the interface between the metal particles and the impact glass in the form of flakes or crescents. The ubiquitous presence of multiphase reaction products indicates that oldhamite is not an original material from foreign objects such as meteorites, but a product generated in situ. CaO can remove S from high-temperature metal solutions, which has been widely exploited in metallurgical engineering[39,40]. In lunar soil, metal sulfides and metal phases are commonly found in Ca-rich glass (rich in anorthite), but oldhamite has not been found to date[37]. This suggests that the formation of oldhamite is different from that of a widespread impact event[7].

As shown in Fig. 4e, g and Supplementary Fig. 5, in the HAADF of the oldhamite crystals of the Chang'E-6 lunar soil, there are bright areas and dark areas with different contrasts. Through EELS, it can be found that in the bright area, there is a detectable Fe $L_{2,3}$ edge peak, while there is almost no Fe in the glass matrix and dark area. At the same time, as shown in Fig. 4h–j, Supplementary Fig. 6, when the

https://doi.org/10.1038/s41467-025-57337-0

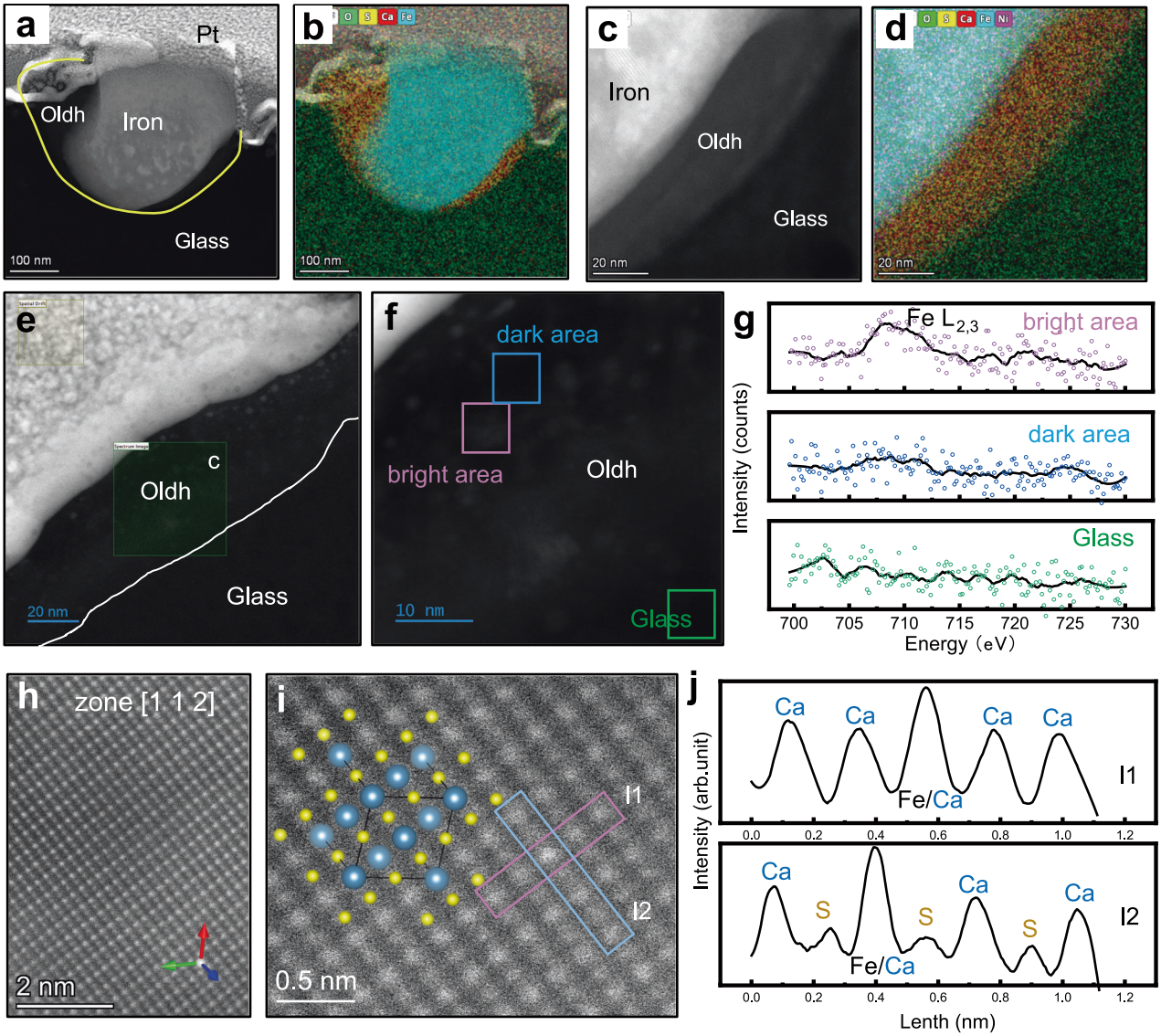

Fig. 4 | Interface chemical composition and crystal doping of oldhamite in the Chang'E-6 lunar soil. a–d HAADF and EDS mapping results of oldhamite (Oldhamite marked as Oldh); **e–g** HAADF images and Fe $L_{2,3}$ edge EELS of Iron particles fall off oldhamite (The pink box refers to the bright area, the blue box refers to the dark area, and the green box refers to the glass, corresponding to the same color curve in (**g**)). **h–j** Atomic-level HAADF image of Ca and S layers and line-scan grayscale image of oldhamite (L1 and L2 in (**i**) refer to the direction of the grayscale image in (**j**); The blue sphere is Ca and the yellow sphere is S).

incident electron beam is in the [1 1 2] direction, Ca atoms and S atoms occupy two layers under HAADF, and atoms with larger atomic numbers can be found in the atomic phase to replace the position of Ca. Combined with the EELS results, the heavy atoms should be Fe. The phase relationship of the iron-oldhamite phase interface also suggests a connection between the two causes (Supplementary Fig. 7). Fe (metal phase) participates in the formation process of oldhamite, which is related to the diffusion of elemental iron particles. It indicates that in addition to the Ca ions in the glass, the iron in the metal phase also contributes a small amount of cations to oldhamite. This shows that oldhamite is formed in the interface reaction between metal-rich phase and Ca-containing glass.

The formation mechanism of Chang'E-6 lunar soil oldhamite

Oldhamite s mainly observed in enstatite meteorites, coexisting with other condensate minerals in calcium-aluminum-rich inclusions or forming complex sulfide-metal nodules[41]. In these systems, oldhamite may indicate high-temperature gas phase reactions in the early nebula stage or large impact events[30,42–44]. Mercury or sulfide-rich asteroids in our solar system may be rich in oldhamite[45,46] because the surface of Mercury is covered with an atmosphere rich in sulfur. The high temperature of impact environments provides favorable conditions for the formation of oldhamite, and observational evidence has obtained[46,47]. Oldhamite may also be widely present in asteroids rich in metals and sulfides, such as Psyche[48]. Lunar studies have shown that oldhamite may exist in the lunar mantle and has a unique isotope fractionation process[49]. Simulation experiments and theoretical calculations have also reproduced oldhamite in the laboratory, indicating it forms under high temperatures and high pressure[31,50]. However, the impact glass rich in metal sulfide particles is easily observed in the lunar soil, this indicates that widespread impact events will not lead to the formation of oldhamite, and the formation of oldhamite requires additional conditions.

As shown in Fig. 5a (and Supplementary Figs. 8–11), oldhamite is characterized in detail. From the EDS-mapping of the S and Fe elements, it can be found that the dissolution of the S and Fe elements in the glass is found near the oldhamite crystal. The area where S dissolves is directly below the metal iron phase, indicating that the S

https://doi.org/10.1038/s41467-025-57337-0

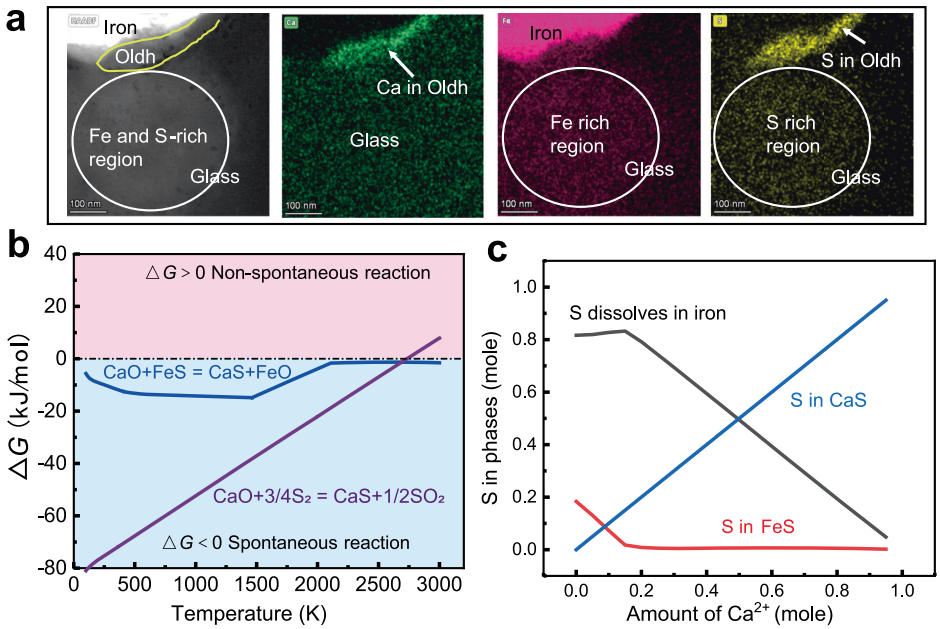

Fig. 5 | Sample evidence and thermodynamic calculations of the by-products of the oldhamite formation reaction. a HAADF and EDS mapping of the Fe and S-rich region near oldhamite in impact glass (Oldhamite is labeled as Oldh; the solid yellow line indicates the Oldh area, and the white circles indicate the Fe- and S-rich region; in EDS-mapping, green is Ca, pink is Fe, and yellow is S); **b** Gibbs free energy criterion for possible reactions of characteristic products in oldhamite system (The blue curve and purple curve are the Gibbs free energies corresponding to different chemical reactions, and the pink background and blue background are the areas where the Gibbs free energy is greater than and less than 0, respectively.); **c** Thermochemical equilibrium calculation of S element with gradual addition of Ca^{2+} ions in the system (The curves corresponding to the fonts of different colors represent the physical phases of the S element distribution.).

element may come from the metal phase. Therefore, the phase of the product can be summarized oldhamite exists between the metallic iron phase and the impact glass in a crescent shape, and a Fe and S-rich region can be found near the impact glass. This suggests that the S in the glass may come from FeS, and the glass with Fe components is also a by-product. The source of S in oldhamite also comes from the metal phase. FeS and the dissolved S in the metal phase may be the key sources of S, while Ca can only come from CaO in the impact glass. Therefore, combined with the evidence found, the chemical reaction formula for the production of oldhamite may be: $CaO_{(melt)} + 3/4S_{2(metal)} = CaS_{(Oldh)} + 1/2SO_{2(g\ or\ melts)}$ and $CaO_{(melt)} + FeS_{(metal)} = CaS_{(Oldh)} + FeO_{(melt)}$. Combined with the theoretical calculation of chemical thermodynamics, as shown in Fig. 5b, c (and Supplementary Figs. 12–15), the Gibbs free energy criterion of the reaction allows the chemical reaction to proceed. From the distribution of multiple phases of the S element (Fig. 5c), CaS phase has the highest S distribution priority. From the perspective of phase equilibrium and gas phase redox degree (Supplementary Fig 12), in the temperature range of 1500 K–3000 K, there is a stable zone where CaS and Fe coexist. The higher the temperature, the smaller the required P_S/P_O ratio (that is, $P_S/P_O \approx 10^4$; at 2000 K, $P_S/P_O \approx 10^3$; at 2500 K, $P_S/P_O \approx 10^2$; at 3000 K, $P_S/P_O \approx 10^{1\text{-}2}$.). From the evidence of CaO activity in lunar soil glass (Supplementary Figs. 13–15), the higher the temperature, the higher the activity of CaO (2000 K ≈ 0.01,3000 K ≈ 0.1). When the temperature over 2500 K in the anorthite system, the activity of CaO can realize the chemical reaction. Therefore, the formation of oldhamite may require temperature over 2500 K, with a higher P_S and a lower P_O. This indicates that a large impact or excavation rich in S components occurred near the Chang'E-6 lunar soil sampling area.

Since the reduced condition is not common on the Moon, the existence of oldhamite should represent a unique event or period over the Moon's history. Based on the simulation above, we infer the formation of oldhamite may have occurred as follows: (1) It may have been produced by a large impact caused by an S-rich impact body, which is similar to the large impact produced on the surface of S-rich asteroids. The high temperature and long insulation time of the large impact caused metals and sulfides exchange elements with the high-temperature impact glass; (2) It may have been produced by excavation and thermal events that reached the scale of the lunar S-rich mantle-core impact (or SPA impact). The excavation could have been caused by large impacts and extensive thermal events formed by ultra-high temperature chemical reactions of S-rich components of the lunar core[51] or lunar mantle[19]. Regardless of which formation mechanism occurred, the oldhamite was likely generated by high-temperature multiphase reactions caused by an impact event since it was discovered at the junction of two phases (metal and oxide), indicating the diversity of the source of Chang'E-6 lunar soil and the complexity of the thermal environment.

Methods

CE6C0300YJFM001

The Chang'E-6 lunar samples CE6C0300YJFM001 investigated in this study were scooped from the surficial lunar regolith. The samples were extracted from a larger sample in a glove box under high-purity argon gas. We selected the fine fraction and spread the material on a silicon wafer coated with a gold film for scanning electron microscopy (SEM) observations.

FIB-SEM

The morphology and composition of the grain with troilite were analyzed using an FEI Scios field-emission scanning electron microscope equipped with energy-dispersive X-ray spectrometers. We selected regions to obtain thin slices (~100 nm thick) using an FEI Scios dual-beam system.

TEM-EELS

The FIB slices were examined using field-emission TEM (200 kV, FEI Talos F200X) to determine the morphology of the troilite. The chemical composition and crystal structure were acquired using TEM-EDS and selected-area electron diffraction (SAED) patterns.

EELS was employed to acquire atomic images of troilite and magnetite and measure the oxidation state of Fe in the two minerals. The detection was performed using a Thermofisher Spectra 300 instrument operating at an accelerating voltage of 300 kV. We obtained the EELS spectra using a Dual-EELS instrument with a probe current of 20 pA and a Gatan 1065 K3 EELS receiver. We used an exposure time of 0.00034 s and tested the samples for 10 cycles to ensure the accuracy of the results of the light elements (O, S). The full width at half maximum (FWHM) of the calibrated zero-loss peak (ZLP) was 0.7 eV to achieve a high energy resolution.

Thermodynamic calculations

The thermodynamic equilibrium, the Gibbs free energy, and the enthalpy change of the chemical reaction between Ca and FeS were obtained using the equilibrium module and chemical reaction module of the Factsage8.0 thermodynamic calculation software. We derived the transition of the system equilibrium for different amounts of Ca in the iron-sulfur system at a temperature of 2273 K. The reaction module was used to calculate the Gibbs free energy change and enthalpy change of the chemical reaction of CaO and FeS、S_2 at different temperatures under standard conditions. The Gibbs free energy change indicates the spontaneity of the reaction, and the enthalpy change indicates the endothermic and exothermic properties of the reaction. The ternary phase diagram and the dominant region diagram are also drawn using the same initial conditions.

Data availability

The source data generated in this study have been deposited in the Mendeley Data under accession code "https://doi.org/10.17632/khvrxvj27c.1".

References

1. Wang, Y. et al. A catalogue of impact craters and surface age analysis in the Chang'e-6 landing area. *Remote Sens.* **16**, 2014 (2024).
2. Li, C. et al. Nature of the lunar farside samples returned by the Chang'E-6 mission. *Natl. Sci. Rev.* **11**, nwae328 (2024).
3. Yue, Z. et al. Geological context of the Chang'e-6 landing area and implications for sample analysis. *Innovation* **5**, 100663 (2024).
4. Qian, Y. et al. Long-lasting farside volcanism in the Apollo basin: Chang'e-6 landing site. *Earth Planet. Sci. Lett.* **637**, 118737 (2024).
5. Zeng, X. et al. Landing site of the Chang'e-6 lunar farside sample return mission from the Apollo basin. *Nat. Astron.* **7**, 1188–1197 (2023).
6. Pang, R. et al. New Occurrence of Seifertite and Stishovite in Chang'E-5 Regolith. *Geophys. Res. Lett.* **49**, 2022gl098722 (2022).
7. Anand, M. et al. Space weathering on airless planetary bodies: clues from the lunar mineral hapkeite. *Proc. Natl. Acad. Sci.* **101**, 6847–6851 (2004).
8. Sasaki, S., Nakamura, K., Hamabe, Y., Kurahashi, E. & Hiroi, T. Production of iron nanoparticles by laser irradiation in a simulation of lunar-like space weathering. *Nature* **410**, 555–557 (2001).
9. Guo, Z. et al. Vapor-deposited digenite in Chang'e-5 lunar soil. *Sci. Bull.* **68**, 723–729 (2023).
10. Xian, H. et al. Ubiquitous and progressively increasing ferric iron content on the lunar surfaces revealed by the Chang'e-5 sample. *Nat. Astron.* **7**, 280–286 (2023).
11. Li, C. et al. Impact-driven disproportionation origin of nanophase iron particles in Chang'e-5 lunar soil sample. *Nat. Astron.* **6**, 1156–1162 (2022).
12. Xu, J. et al. Space weathering effects and potential spectral alteration on Phobos and the Moon: Clues from the Fe content of olivine. *Astron. Astrophys.* **672**, A115 (2023).
13. Gu, L. et al. Space weathering of the Chang'e-5 lunar sample from a mid-high latitude region on the moon. *Geophys. Res. Lett.* **49**, e2022GL097875 (2022).
14. Guo, Z. et al. Sub-microscopic magnetite and metallic iron particles formed by eutectic reaction in Chang'E-5 lunar soil. *Nat. Commun.* **13**, 7177 (2022).
15. Guo, Z. et al. Nanophase iron particles derived from fayalitic olivine decomposition in Chang'E-5 lunar soil: implications for thermal effects during impacts. *Geophys. Res. Lett.* **49**, e2021GL097323 (2022).
16. Matsumoto, T. et al. Space weathering of iron sulfides in the lunar surface environment. *Geochim. et. Cosmochim. Acta* **299**, 69–84 (2021).
17. Jones, M. J. et al. A South Pole–Aitken impact origin of the lunar compositional asymmetry. *Sci. Adv.* **8**, eabm8475 (2022).
18. James, P. B. et al. Deep structure of the lunar South Pole-Aitken basin. *Geophys. Res. Lett.* **46**, 5100–5106 (2019).
19. Papike, J., Taylor, L. & Simon, S. Lunar minerals. *Lunar sourcebook: A user's guide to the Moon*, 121-181 (1991).
20. Frost, B. R., Mavrogenes, J. A. & Tomkins, A. G. Partial melting of sulfide ore deposits during medium-and high-grade metamorphism. *Can. Mineral.* **40**, 1–18 (2002).
21. Juza, R. & Bünzen, K. Untersuchungen über das system calcium-carbid/calciumsulfid. *Z. f.ür. Physikalische Chem.* **17**, 82–99 (1958).
22. Haberle, C. W. & Garvie, L. A. Extraterrestrial formation of oldhamite and portlandite through thermal metamorphism of calcite in the Sutter's Mill carbonaceous chondrite. *Am. Mineral.* **102**, 2415–2421 (2017).
23. Piani, L., Marrocchi, Y., Libourel, G. & Tissandier, L. Magmatic sulfides in the porphyritic chondrules of EH enstatite chondrites. *Geochim. et. Cosmochim. Acta* **195**, 84–99 (2016).
24. Keil, K. Mineralogical and chemical relationships among enstatite chondrites. *J. Geophys. Res.* **73**, 6945–6976 (1968).
25. Jacquet, E., Alard, O. & Gounelle, M. The formation conditions of enstatite chondrites: insights from trace element geochemistry of olivine-bearing chondrules in Sahara 97096 (EH 3). *Meteorit. Planet. Sci.* **50**, 1624–1642 (2015).
26. Floss, C. & Crozaz, G. Heterogeneous REE patterns in oldhamite from aubrites: their nature and origin. *Geochim. et. Cosmochim. Acta* **57**, 4039–4057 (1993).
27. Defouilloy, C., Cartigny, P., Assayag, N., Moynier, F. & Barrat, J.-A. High-precision sulfur isotope composition of enstatite meteorites and implications of the formation and evolution of their parent bodies. *Geochim. et. Cosmochim. Acta* **172**, 393–409 (2016).
28. Lundberg, L. L., Zinner, E. & Crozaz, G. Search for isotopic anomalies in oldhamite (CaS) from unequilibrated (E3) enstatite chondrites. *Meteoritics* **29**, 384–393 (1994).
29. El Goresy, A. et al. Origin of EL 3 chondrites: evidence for variable C/O ratios during their course of formation—a state of the art scrutiny. *Meteorit. Planet. Sci.* **52**, 781–806 (2017).
30. Larimer, J. W. An experimental investigation of oldhamite, CaS; and the petrologic significance of oldhamite in meteorites. *Geochim. et. Cosmochim. Acta* **32**, 965–982 (1968).
31. Liu, Y. et al. Oldhamite: a new link in upper mantle for C–O–S–Ca cycles and an indicator for planetary habitability. *Natl Sci. Rev.* **10**, nwad159 (2023).
32. Martinez, M., Meen, J. & Barker, D. Lunar soil sample 74221, 2–A study of unusual fines. *Environ* **2**, 3 (2019).
33. Mokhov, A. V. et al. Fluorite, hatchettolite, calcium sulfate, and bastnasite-(Ce) in the lunar regolith from Mare Crisium. *Dokl. Earth Sci.* **422**, 1178–1180 (2008).
34. Pang, R. et al. Redox condition changes caused by impacts: insights from Chang'e-5 lunar glass beads. *Sci. Bull.* **69**, 1495–1505 (2024).
35. Li, C. et al. Characteristics of the lunar samples returned by Chang'E-5 Mission. *Natl. Sci. Rev.* **9**, nwab188 (2022).
36. Yan, P. et al. Submicroscopic iron-rich grains throughout impact glasses in Chang'E-5 regolith. *Icarus* **410**, 115920 (2024).

37. Li, C. et al. Impact-dispersed Fe–Fe1− xS core–shell particles in Chang'e-5 lunar soil impact glass. *Geochim. et. Cosmochim. Acta* **379**, 134–144 (2024).
38. Cymes, B. A., Burgess, K. D. & Stroud, R. M. Helium reservoirs in iron nanoparticles on the lunar surface. *Commun. Earth Environ.* **5**, 189 (2024).
39. Shi, C.-b, Huang, Y., Zhang, J.-x, Li, J. & Zheng, X. Review on desulfurization in electroslag remelting. *Int. J. Miner, Metall. Mater.* **28**, 18–29 (2021).
40. Visuri, V.-V., Vuolio, T., Haas, T. & Fabritius, T. A review of modeling hot metal desulfurization. *Steel Res. Int.* **91**, 1900454 (2020).
41. Dai, W., Moynier, F. & Siebert, J. Insights on the origin of oldhamite in enstatite meteorites from Ca stable isotopes. *Geochim. et. Cosmochim. Acta* **375**, 247–257 (2024).
42. Crozaz, G. & Lundberg, L. L. The origin of oldhamite in unequilibrated enstatite chondrites. *Geochim. et. Cosmochim. Acta* **59**, 3817–3831 (1995).
43. Guan, Y., Huss, G. R., MacPherson, G. J. & Wasserburg, G. J. Calcium-aluminum-rich inclusions from enstatite chondrites: indigenous or foreign? *Science* **289**, 1330–1333 (2000).
44. Rubin, A. E. Mineralogy of meteorite groups. *Meteorit. Planet. Sci.* **32**, 231–247 (1997).
45. Wheelock, M., Heavilon, C., Keil, K., Taylor, G. & Crozaz, G. Coarse-grained oldhamite in an igneous clast in the Norton County aubrite: REE measurements. *Meteoritics* **24**, 340 (1989).
46. Carli, C. et al. Laboratory emissivity spectra of sulphide-bearing samples, new constraints for the surface of Mercury: oldhamite in mafic aggregates. *Minerals* **14**, 62 (2024).
47. Burbine, T. H. et al. Spectra of extremely reduced assemblages: implications for Mercury. *Meteorit. Planet. Sci.* **37**, 1233–1244 (2002).
48. Bell, J. et al. The Psyche multispectral imager investigation: characterizing the geology, topography, and compositional properties of a metallic world. *Lunar Planet. Sci. Conf.* **1903**, 1366 (2016).
49. Huang, F., Zhou, C., Wang, W., Kang, J. & Wu, Z. First-principles calculations of equilibrium Ca isotope fractionation: Implications for oldhamite formation and evolution of lunar magma ocean. *Earth Planet. Sci. Lett.* **510**, 153–160 (2019).
50. Larimer, J. W. & Ganapathy, R. The trace element chemistry of CaS in enstatite chondrites and some implications regarding its origin. *Earth Planet. Sci. Lett.* **84**, 123–134 (1987).
51. Brett, R. A lunar core of Fe-Ni-S. *Geochim. et. Cosmochim. Acta* **37**, 165–170 (1973).

Acknowledgements

We thank CNSA for providing access to the Lunar samples NO. CE6C0300YJFM001. The authors also acknowledge funding support from the National Natural Science Foundation of China Young Scientist Fund (No.42403043) to L.C.Youth Innovation Promotion Association, Chinese Academy of Sciences (2020395) to L.Y., Strategic Priority Research Program of the Chinese Academy of Sciences grant XDB 41000000 to L.J.Z., National Natural Science Foundation of China (42273042 and 41931077) to L.Y., "From 0 to 1" Original Exploration Cultivation Project, Institute of Geochemistry, Chinese Academy of Sciences (DHSZZ2023-3) to L.Y.

Author contributions

L.C. analyzed the datasets and wrote the manuscript. P.R.H. and H.Z.X. contributed to the data discussion. L.C., X.J.Y., W.Y.Y., H.W.B., Y.J., H.Z.X., W.L. and Q.Z.Y. completed testing and sample sorting. L.C., L.Y., Z.X.J., and M.W.H. contributed to the experimental design and manuscript discussion. L.X.Y., L.J.Z., and M.W.H. contributed to the manuscript discussions.

Competing interests

The authors declare no competing interests.

Additional information

Supplementary information The online version contains supplementary material available at https://doi.org/10.1038/s41467-025-57337-0.

Correspondence and requests for materials should be addressed to Yang Li.

Peer review information *Nature Communications* thanks Wei Dai and the other, anonymous, reviewer for their contribution to the peer review of this work. A peer review file is available.